

# A Survey of UV Bright Sources Behind the Halo of M31

Andrew Fittingoff<sup>1</sup>, J. Xavier Prochaska<sup>1,2</sup>, Jasonjot S. Kalirai<sup>2,3</sup>, Jay Strader<sup>1,4,5</sup>  
 Puragra Guhathakurta<sup>1,2</sup>, Kyle F. Kaplan<sup>1</sup>

<sup>1</sup>*Department of Astronomy and Astrophysics, University of California, Santa Cruz, CA 95064.*

<sup>2</sup>*University of California Observatories - Lick Observatory, University of California, Santa Cruz, CA 95064*

<sup>3</sup>*Space Telescope Science Institute, Baltimore, MD, 21218*

<sup>4</sup>*Harvard-Smithsonian Center for Astrophysics, Cambridge, MA 02138*

<sup>5</sup>*Hubble Fellow*

15 July 2009

## ABSTRACT

We have performed a wide-area ultraviolet (UV) imaging survey using the GALaxy Evolution eXplorer (GALEX) to search for bright, point-like UV sources behind M31’s extended halo. Our survey consisted of 46 pointings covering an effective area of  $\approx 50\text{deg}^2$ , in both the far-UV and near-UV channels. We combined these data with optical *R*-band observations acquired with the WIYN Mosaic-1 imager on the Kitt Peak National Observatory 0.9m WIYN telescope. An analysis of the brightness and colors of sources matched between our photometric catalogs yielded  $\approx 100$  UV-bright quasar candidates. We have obtained discovery spectra for 76 of these targets with the Kast spectrometer on the Lick 3m telescope and confirm 30 active galactic nuclei and quasars, 29 galaxies at  $z > 0.02$  including several early-type systems, 16 Galactic stars (hot main-sequence stars), and one featureless source previously identified as a BL Lac object. Future UV spectroscopy of the brightest targets with the Cosmic Origins Spectrograph on the Hubble Space Telescope will enable a systematic search for diffuse gas in the extended halo of M31.

**Key words:** galaxies: haloes – galaxies: individual: M31 – quasars: absorption lines

## 1 INTRODUCTION

Structure formation, in current cosmology, follows from the gravitational collapse of dark matter into virialized ‘halos’. Modern theory also predicts that diffuse baryons are pulled along during the collapse. A subset of these may travel to the center of the dark matter halo, dissipate their internal energy, and condense further to form stars. A significant fraction, however, may instead be shock-heated to the virial temperature of the dark matter halo to form a hot, diffuse baryonic halo. Modern cosmological simulations suggest that the amount of baryons that travel along these two paths is a sensitive function of the total mass, dark matter halo mass, and also the age of the universe (Kereš et al. 2005; Dekel et al. 2008). Independent of gravitational heating, feedback processes related to galaxy formation (e.g. galactic winds, AGN outflows), galaxy-galaxy interactions (e.g. mergers), and even interactions between galaxies and this diffuse medium (e.g. ram-pressure stripping) may also pollute the halo with diffuse and, possibly, metal-enriched gas. Studies of halo gas, therefore, trace the processes of structure formation and may constrain the roles of feedback in galaxy evolution.

Halo gas is observed in emission from the largest virialized structures of our universe: clusters and groups. Termed the intra-cluster medium (ICM) or intragroup gas, this material emits X-rays via Brehmstrahlung processes that are recorded by space-borne satellites (Forman & Jones 1982; Mulchaey et al. 2003). The ob-

servations assess the temperature, enrichment, and density profiles of this halo gas. In turn, the halo’s gas serves as a vital diagnostic for the potential well of massive dark matter halos. The analysis indicates that the majority of baryons in clusters and massive groups are located within this medium, far surpassing the stellar mass of individual galaxies (e.g. Allen et al. 2008). Indeed, it has been suggested that diffuse halo gas may be the dominant baryonic reservoir in the present-day universe (Mulchaey et al. 1996; Fukugita et al. 1998; Prochaska & Tumlinson 2008).

The most successful approach thus far to studying the halo gas has been through absorption-line studies, i.e. rest-frame ultraviolet spectroscopy of distant quasars whose sightlines coincidentally intersect the projected halos of foreground galaxies. These observations reveal that galactic halos have a multi-phase medium comprised of cool, photoionized material (traced by  $MgII$  absorption; Lanzetta & Bowen 1992; Kacprzak et al. 2007) and a warmer, more diffuse component traced by higher ionization states (e.g.  $CIV$ ,  $OVI$ ; Chen et al. 2001; Tripp et al. 2007). Photoionization modeling of this gas constrains the density, temperature, and metallicity of the gas (e.g. Churchill et al. 2000; Chen & Prochaska 2000). Because of the inefficiencies of UV spectroscopy, the sample sizes have been very modest and only recently have observers been pursuing studies that yield a statistical description for a large population of galaxies by focusing on  $MgII$  transitions redshifted

into optical passbands (Zibetti et al. 2007; Chen & Tinker 2008). Even with this approach, it is extremely rare to study a single halo with more than one sightline. As such, we lack a detailed knowledge of the distribution and properties of gas (neutral or ionized) within individual galactic halos.

The Andromeda spiral galaxy (M31), a nearby massive spiral, is an excellent galaxy for such a study. Its stellar halo is known to extend out to  $\approx 25$  degrees, or  $\approx 150$  kpc (Guhathakurta et al. 2005; Kalirai et al. 2006; Gilbert et al. 2006). M31 is a representative late-type spiral of the present Universe. Furthermore, as our nearest (big galaxy) neighbor there is a large and expanding dataset of supplementary observations including multi-band imaging, high spatial resolution images of select fields, and a tremendous set of optical spectroscopy on individual stars (e.g. Ibata et al. 2007; Guhathakurta et al. 2006; Brown et al. 2007; Gilbert et al. 2007). Regarding the gaseous halo, clouds of hydrogen gas have been sighted in M31 with similar properties as the Galactic HVCs (Thilker et al. 2004). These clouds or their lower column density counterparts are prime targets for spectroscopic analysis throughout the extended halo. Unfortunately, emission studies of warm/hot diffuse gas are challenged by the same foregrounds that preclude studies within the Milky Way. It is a natural extension of our experience with the Galactic halo to consider surveying M31's halo through absorption-line studies. The challenge, however, is to identify bright UV sources behind the halo of M31 and then obtain high fidelity spectroscopy.

With this challenge as our motivation, we initiated a UV/optical survey of  $\approx 50\text{deg}^2$  of M31's galactic halo. In order to maximize our search area for QSO detections, we used the GALaxy Evolution eXplorer (GALEX) telescope (Morrissey & GALEX Science Team 2005). Starting in Cycle 1, the GALEX team began acquiring images of the disk and inner spheroid of M31. These data are complemented by images and spectra from the Sloan Digital Sky Survey. We were granted a Cycle 2 GO project to image the extended halo of M31 with GALEX. This paper reports on these observations and additional optical imaging and spectroscopy for quasar candidate selection and confirmation.

This paper is organized as follows. In § 2, we describe our GALEX Imaging observations of M31's halo. The optical photometry is discussed in § 3 and § 4 details our QSO candidate selection process. In § 5 we present first results from our follow-up, optical spectroscopy and § 6 summarizes the main findings.

## 2 GALEX IMAGING

We were awarded a total of 46 pointings during Cycle 2 (PI: Prochaska; ID=033) of the GALEX mission to image a portion of M31's outer halo. The pointings extend radially outwards from the guaranteed time observations of M31's disk and inner spheroid. We had proposed to image the halo along radial spokes extending to  $\sim 100$  kpc along N, NE, E, SE, S, SW, W, and NW directions. Most of the proposed positions were shifted by several arcminutes to satisfy the GALEX bright star detector limits. Furthermore, only a subset of our requested pointings were actually acquired. These are diagrammed in Figure 1 and listed in Table 1.

The exposure time for each observation was set to one orbit (1631 s). The incoming beam is split by a dichroic into the far-UV (*FUV*; 1350–1790Å) and near-UV (*NUV*; 1770–2730Å) channels. The unvignetted field-of-view of each pointing is a circle with radius  $\approx 35'$  that is imaged simultaneously by two cameras for a to-

**Table 1.** Summary of GALEX pointings.

ID	Date (UT)	$\alpha_{J2000}$	$\delta_{J2000}$
SW4	06 Nov 2005	00:32:24.00	+37:30:00.0
SW5	06 Nov 2005	00:26:57.18	+36:35:59.9
S6	06 Nov 2005	00:42:44.32	+34:39:00.0
SW3	06 Nov 2005	00:33:30.78	+38:05:59.9
S5	06 Nov 2005	00:43:08.32	+35:31:01.1
S4	06 Nov 2005	00:44:24.00	+36:25:01.1
S3	06 Nov 2005	00:42:44.32	+37:31:01.1
SE9	07 Nov 2005	01:13:47.67	+35:24:17.9
SW2	07 Nov 2005	00:37:12.00	+38:31:47.9
W4	08 Nov 2005	00:23:49.22	+41:20:59.9
SE7	08 Nov 2005	01:07:50.55	+36:56:41.9
W6	08 Nov 2005	00:15:18.00	+41:42:54.0
SE11	08 Nov 2005	01:21:07.20	+34:20:59.9
W2	08 Nov 2005	00:24:42.00	+42:27:00.0
W3	08 Nov 2005	00:27:00.00	+41:16:08.4
E3	08 Nov 2005	00:58:24.00	+41:16:08.4
SE2	08 Nov 2005	00:54:47.99	+39:33:53.9
NE2	09 Nov 2005	00:50:33.60	+43:19:48.0
N1	09 Nov 2005	00:42:44.32	+43:22:48.0
E2	09 Nov 2005	00:58:47.99	+42:17:59.9
E6	09 Nov 2005	01:14:24.00	+42:12:00.0
NE3	09 Nov 2005	00:54:47.99	+44:39:00.0
E5	09 Nov 2005	01:06:00.00	+42:12:00.0
N3	09 Nov 2005	00:41:47.99	+45:17:59.9
N2	09 Nov 2005	00:42:44.32	+44:13:47.9
SE12	09 Nov 2005	01:23:43.35	+33:32:41.9
NW6	10 Nov 2005	00:19:49.90	+45:28:08.4
SE14	10 Nov 2005	01:30:04.47	+32:18:18.0
NE6	10 Nov 2005	01:02:35.99	+46:17:59.9
SE13	10 Nov 2005	01:26:53.91	+32:55:29.9
N4	10 Nov 2005	00:41:31.20	+46:12:00.0
NW5	10 Nov 2005	00:25:00.00	+45:12:00.0
NE4	10 Nov 2005	00:54:47.99	+45:09:00.0
NE5	10 Nov 2005	01:04:00.00	+45:17:59.9
NW2	29 Jul 2006	00:30:56.23	+42:40:33.8
NW3	30 Jul 2006	00:28:12.00	+43:15:00.0
W5	30 Jul 2006	00:19:33.80	+41:15:21.8
SW6	30 Jul 2006	00:22:52.38	+36:32:49.2
W7	06 Aug 2006	00:09:36.00	+40:30:00.0
SE1	14 Sep 2006	00:50:00.00	+39:33:53.9
S2	14 Sep 2006	00:43:12.00	+38:11:23.9
SE3	15 Sep 2006	00:55:08.31	+36:55:29.9
SE6	15 Sep 2006	01:03:45.43	+37:15:07.4
E4	15 Sep 2006	01:03:08.76	+40:26:13.4
SE5	19 Sep 2006	01:03:12.00	+38:20:59.9
SE10	19 Sep 2006	01:17:22.23	+34:35:59.9

Note: The ID represents the direction with respect to the center of M31. Each pointing was imaged in NUV and FUV, with an FOV of  $\approx 1.2\text{deg}^2$ .

tal field-of-view (FOV) of approximately  $1.2\text{deg}^2$ . The raw images were processed through the reduction pipeline at the GALEX Science Operations Center<sup>1</sup>. The output image has been background subtracted, flux calibrated, and astrometrically corrected to an accuracy of  $1''$ .

We measured the brightness of all sources on each image, in both filters, using the SExtractor software package (version 2.5.0; Bertin & Arnouts 1996). The full width at half maximum (FWHM) of point sources on each *NUV* image subtends  $\sim 3.2$  pixels. Given

<sup>1</sup> <http://galexgi.gsfc.nasa.gov/docs/galex/Documents/GALEXPipelineDataGuide.pdf>

**Table 2.** PHOTOMETRY SUMMARY OF GALEX/NUV DETECTED SOURCES IN THE HALO OF M31

ID (J2000)	Name (J2000)	$\alpha_{GALEX}$ (AB)	$\delta_{GALEX}$ (AB)	$FUV$ (AB)	$\sigma_{FUV}$ (AB)	$NUV$ (AB)	$\sigma_{NUV}$ (AB)	$R^a$	$\sigma_R$	Class <sup>b</sup>	Cand <sup>c</sup>
1	GALEX J000639.12+402641.2	00:06:39.12	+40:26:41.2	21.50	0.12	20.79	0.05	...	...	0.99	N
2	GALEX J000639.68+402949.3	00:06:39.68	+40:29:49.3	99.99	-1.00	19.54	0.02	...	...	0.98	N
3	GALEX J000640.06+403418.4	00:06:40.06	+40:34:18.4	99.99	-1.00	19.41	0.02	...	...	1.00	N
4	GALEX J000642.73+402405.4	00:06:42.73	+40:24:05.4	99.99	-1.00	22.16	0.10	...	...	1.00	N
5	GALEX J000643.10+402835.3	00:06:43.10	+40:28:35.3	99.99	-1.00	20.78	0.04	...	...	0.98	N
6	GALEX J000644.53+403139.9	00:06:44.53	+40:31:39.9	21.11	0.10	20.60	0.04	...	...	1.00	N

Note: a:  $R$ -band magnitudes from KPNO photometry are reported for the NUV extraction that are matched to within a  $2''$  radius of a KPNO source. For NUV extractions where KPNO imaging exists but no source was detected, we report a value of 99.99 and an error of -1. For NUV extractions where no KPNO imaging exists, we report no values. a: Star/galaxy classifier calculated by SExtractor on the NUV photometry. Values near unity indicate a stellar-like point-spread function. b: Quasar candidates picked based on color relations between UV and R. The criteria used were  $.5 < FUV - NUV < 2$ ,  $NUV - R < 2$ , and  $NUV < 21$ . d: NUV extractions with no FUV match have FUV values of 99.99 and an error of -1. [The complete version of this table is in the electronic edition. The printed edition contains only a sample.]

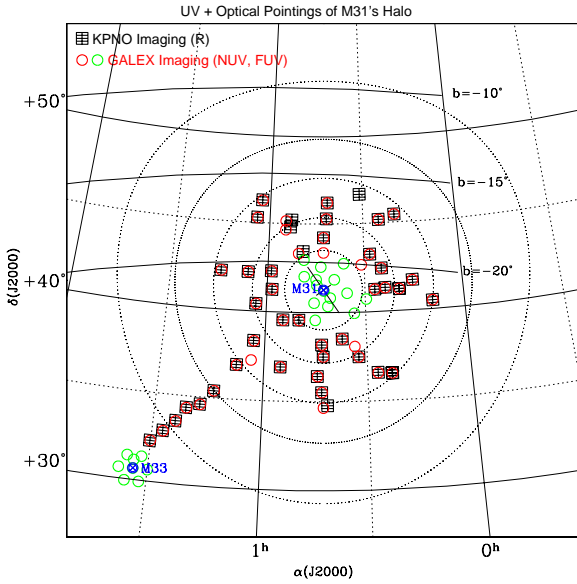


**Figure 1.** Diagram of our Cycle 2 GALEX and our KPNO MOSA pointings with respect to M31 (GALEX are circles, KPNO are squares). Pointings were shifted around to avoid exceptionally bright objects that could damage GALEX's sensitive instruments. The GTO GALEX observations include several pointings on the disk of M31 that have also been imaged by the Sloan Digital Sky Survey. These fields were not included in our program which targets M31's halo.

the pixel scale of the detector ( $1.5''$  pixel<sup>-1</sup>), the angular FWHM is  $4.8''$  (the FWHM for the  $FUV$  exposures is slightly smaller at  $4.2''$ ). The aperture size was set to the FWHM, and each source with counts more than  $\sim 3\sigma$  above the mean local sky-subtracted background was considered a detection. The resulting catalog included a large number of artifacts at the circular edges of each image. We trimmed the catalogs to only include a fraction of the total radius, i.e.  $0.5625$  deg from the center (1325 pixels) giving a total area  $0.994$  deg<sup>2</sup> for each field. This resulted in a total number of 102385 objects in the combined  $NUV$  data. Approximately  $\sim 15\%$  of the sources were also detected at  $3\sigma$  significance in the  $FUV$  images. The sources that were undetected in the  $FUV$  images were retained in the final catalogs but flagged to note that a precise  $FUV - NUV$  color is not available. The sources with-

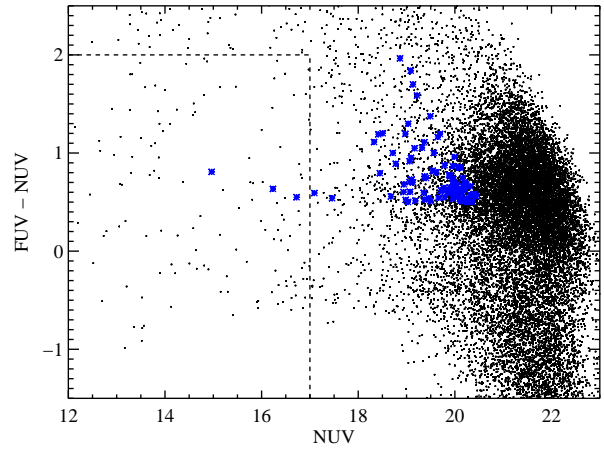


**Figure 2.** Color-magnitude diagram of all GALEX objects. Our initial criteria for picking out QSOs was to look for bright  $NUV$  magnitudes and blue  $FUV - NUV$  color (within the box on the diagram). Follow-up spectroscopy indicates that a very high fraction of these sources are foreground Galactic stars. As such, we obtained KPNO optical imaging of the fields to perform more efficient color-color pre-selection. The blue stars indicate the position of these preferred candidates in the  $NUV/FUV$  color-magnitude diagram.

out significant  $FUV$  flux are unlikely to correspond to UV-bright sources background to M31. The fixed-aperture photometry for all sources detected in the  $NUV$  band is presented in Table 2.

The reduced images from the GALEX pipeline record the data in flux units where one digital number (DN) corresponds to  $1.4 \times 10^{-15}$  erg s<sup>-1</sup> cm<sup>-2</sup> Å<sup>-1</sup> for the  $FUV$  images and  $2.06 \times 10^{-16}$  erg s<sup>-1</sup> cm<sup>-2</sup> Å<sup>-1</sup> for the  $NUV$  images. The conversion from flux to AB magnitudes for GALEX data is given by<sup>2</sup>

$$M_{FUV} = 18.82 - 2.5 * \log(DN) \quad (1)$$

$$M_{NUV} = 20.08 - 2.5 * \log(DN) \quad (2)$$

where 18.82 and 20.08 are the corresponding zero point AB magnitudes. A color magnitude diagram of all  $\approx 17,000$  sources detected in both filters in our survey is presented in Figure 2.

<sup>2</sup> <http://www.galex.caltech.edu/researcher/techdoc-ch2.html>

**Table 3.** Log of KPNO Observations.

ID	Date (UT)	$\alpha_{J2000}$	$\delta_{J2000}$	FWHM (pix)
N2	25 Nov 2006	00:42:43.82	44:13:51.18	2.1
N3	25 Nov 2006	00:41:47.79	45:18:04.08	2.2
N4	25 Nov 2006	00:41:30.95	46:12:03.05	2.1
NW2	25 Nov 2006	00:30:56.26	46:40:35.03	2.1
NW3	25 Nov 2006	00:28:12.22	43:15:04.82	2.1
NW5	25 Nov 2006	00:25:00.27	45:12:02.60	2.2
NW6	25 Nov 2006	00:19:50.17	45:28:11.29	2.1
W2	25 Nov 2006	00:24:42.47	42:27:05.58	2.2
W3	25 Nov 2006	00:27:00.63	41:16:16.73	2.5
W4	25 Nov 2006	00:23:49.94	41:21:06.52	2.4
W5	25 Nov 2006	00:19:34.69	41:15:28.28	2.3
W5	25 Nov 2006	00:19:32.88	41:15:29.22	2.0
W6	25 Nov 2006	00:15:18.02	41:43:00.03	2.1
W7	25 Nov 2006	00:09:36.34	40:30:06.84	2.0
SW2	25 Nov 2006	00:37:12.29	38:31:56.55	1.7
SW4	25 Nov 2006	00:32:24.28	37:30:10.10	1.7
SW5	25 Nov 2006	00:26:57.67	36:36:10.68	1.4
SW6	25 Nov 2006	00:22:52.89	36:32:59.41	1.5
SW6	25 Nov 2006	00:22:56.29	36:33:06.41	1.9
SW2	25 Nov 2006	00:22:56.29	36:33:06.41	1.8
S2	25 Nov 2006	00:43:17.61	38:11:48.18	2.0
S3	25 Nov 2006	00:42:49.96	37:31:27.13	2.0
S4	25 Nov 2006	00:44:29.66	36:25:28.32	1.8
S5	25 Nov 2006	00:43:14.14	35:31:31.18	1.8
SE1	25 Nov 2006	00:50:06.02	39:34:20.02	1.7
SE2	25 Nov 2006	00:54:54.16	39:34:19.68	1.6
SE3	25 Nov 2006	00:55:14.42	36:55:59.73	1.9
E2	25 Nov 2006	00:58:54.44	42:18:25.27	1.9
SE5	25 Nov 2006	01:03:18.28	38:21:27.97	1.6
SE7	25 Nov 2006	01:07:56.74	36:57:11.77	2.0
SE9	25 Nov 2006	01:13:53.69	35:24:48.86	1.8
E6	25 Nov 2006	01:14:30.60	42:12:24.98	1.7
SE11	25 Nov 2006	01:21:13.28	34:21:31.33	2.0
SE12	25 Nov 2006	01:23:49.48	33:33:13.89	1.7
SE13	25 Nov 2006	01:27:00.06	32:56:03.59	1.8
SE14	25 Nov 2006	01:30:10.64	32:18:52.31	1.8
S6	28 Nov 2006	00:41:33.84	34:47:32.00	1.7
NE2	28 Nov 2006	00:49:09.75	43:26:47.30	1.5
NE3	28 Nov 2006	00:53:17.98	44:49:43.30	1.8
NE4	28 Nov 2006	00:52:58.79	45:13:39.10	1.4
E3	28 Nov 2006	00:58:29.82	41:16:30.15	2.0
E4	28 Nov 2006	01:03:14.52	40:26:35.91	1.9
E5	28 Nov 2006	01:06:05.88	42:12:21.39	1.6
NE6	28 Nov 2006	01:02:42.45	46:18:18.82	2.0
NE5	28 Nov 2006	01:04:06.49	45:18:20.05	1.9
SE10	28 Nov 2006	01:17:27.75	34:36:28.51	2.0

Note: The ID represents the direction with respect to the center of M31. Observations were taken with an R-band filter (6200-7500 Å) with an  $\approx .93\text{deg}^2$  FOV and an exposure time of 60s. The pointings are intended to overlap with the data we received from GALEX. The FWHM values were estimated from the images directly.

### 3 KPNO IMAGING

To increase the efficiency of selecting quasar candidates, we chose to extend our baseline to include optical photometry in the *R*-band (e.g. Atlee & Gould 2007). Although our GALEX data revealed many thousands of bright and blue UV sources, these data by themselves do not provide an efficient means of selecting quasar candidates. We acquired *R*-band images using the WIYN Mosaic-1 imager on the KPNO 0.9 meter WIYN telescope. This section de-

scribes the observations, data reduction, and analysis of these images.

#### 3.1 Image Reduction

On the nights of 25–28 November 2006, we acquired 43 *R*-band images covering nearly the entire area of our GALEX imaging program. We used the WIYN Mosaic-1 imager which records the data in a mosaic of eight CCDs, each one with a viewing area of  $14.49' \times 28.97'$  ( $0.43'' \text{ pixel}^{-1}$ ). Therefore, each mosaic image has a total area of  $\approx .93\text{deg}^2$ , similar to each of our GALEX images. A single Mosaic-1 frame overlapping each GALEX image was obtained with an exposure time of 60 seconds. The nights were relatively clear but thin cirrus precludes precise photometric calibration from standard star fields observed during this run. The seeing ranged from 1 to  $2''$ , and the airmass was  $< 1.6$  for all observations.

The *R* band images were reduced using standard IRAF tasks in the **mscred** module. We first calculated coefficients for each chip of the mosaic data to account for cross-talk between adjacent CCDs. We applied the bad pixel masks, and then subtracted a mean bias frame from each of the raw images. Finally, we corrected for pixel-to-pixel variations by dividing the images by a combined dome flat field. The resulting images, over the full mosaic, showed significant sky gradients caused by spatial and temporal variations in our sky flats. To remove the gradients, we used the IRAF task **mscskysub** to fit a surface to each CCD and subtract the mean background value. In this process, the subtraction ignored large residuals which represent actual objects on the images. The **mscskysub** task is typically used to smooth out the background sky after stitching together individual CCDs to create a large mosaic image. Although we executed this task on individual chips, we checked and confirmed that the photometry derived from the images with and without this processing showed very little difference ( $< 10\%$ ) in the results, provided one performs local sky subtraction. Cosmic rays were not removed or flagged, but the images were short exposures and therefore would have a small contamination rate.

#### 3.2 Astrometry and Photometry

We measured the positions and magnitudes of all sources separately on each of the eight CCDs of the mosaic. Because our observational design consists of a single exposure of each field, this leads to 368 total sub-images. The world coordinate system information recorded in the image headers was systematically in error. We therefore submitted each of the 368 images to Astrometry.net (Hogg et al. 2008) to yield a better estimate of the field center and overall solution. The resulting solution provided an adequate fit over most of the field of view, but some residual mismatch was still seen towards the corners of the chips. The solution was iterated using the **wcstools** module within IRAF by matching only a subset of the brightest, well measured stars to the USNO-B1.0 catalog. The fitting function was a quadratic polynomial after the initial offsets, scales, and rotations were calculated. Recentering of the image center was allowed, as well as sigma clipping of objects that were more than  $2\sigma$  from the expected location based on the previous fit. For the best frames, the rms residual of the solution was less than  $0.3''$  based on several dozen guide stars. For a few of the frames, less than 10 stars were found in common between our catalog and the USNO and we could not recover a useful astrometric solution; these frames were ignored in all subsequent analysis.

Point-spread function (PSF) photometry was performed on each processed image using DAOPHOT and ALLSTAR (Stetson 1994). As the seeing varied from  $1''$  to  $2''$  during the observing run, the fitting radius was set separately for each image to be 80% of the image FWHM. This was measured using the **imexam** IRAF task for a number of bright, isolated, non-saturated stars (see Table 3). All sources more than  $3\sigma$  above the local background were considered positive detections. A PSF template was calculated using  $\sim 50$  bright stars on each frame, and fit to and subtracted from each source to create a residual image. A second pass of the photometry was made on this residual image to yield the final catalog.

We calibrated the magnitudes by comparing to the USNO catalog, which has an  $R$  magnitude and a  $B - R$  color. The overlap between our optical source catalog and the USNO catalog ranged from  $R = 10$  to 19. We fit for a color term and offset for each CCD individually, after applying a cut to eliminate outliers that were more than  $2\sigma$  from the mean. We note that the offsets varied by several tenths of a magnitude for different CCDs. We found that the typical limiting magnitude for our  $3\sigma$  detection criterion is  $R \approx 20$ . The  $R$ -band photometry of all KPNO sources that were matched to a GALEX  $NUV$  detection are listed in Table 2.

## 4 QSO CANDIDATES

### 4.1 Catalog Combination

Our total catalog of GALEX detections via SExtractor, after eliminating duplicates, contained 98629 objects, which were determined by detection in the  $NUV$ . Duplicate detections were chosen to be within  $0.5''$ , and the magnitudes taken from the entry with the smallest error. Objects without a corresponding  $FUV$  detection were given a magnitude value of 99.99 and an error of -1. The total KPNO catalog, after eliminating erroneous detections, totalled 144,531 objects. To find matches between the catalogs we tested for the nearest object within  $1.5''$ . The matched GALEX+KPNO catalog contained 39437 objects. Given the low source density of objects in our relatively shallow  $R$ -band images, we estimate that the number of spurious matches is fewer than 200.

### 4.2 Candidates

The criteria we used to define a quasar candidate list were taken from previous papers on QSO detections using a combination of GALEX and optical data (Bianchi & et al. 2007; Atlee & Gould 2007). The general approach is to take the area in color-color space which maximizes the density of QSOs while minimizing contaminants. QSO colors that include GALEX observations have been measured using the SDSS database. The selections fall into an area defined by searching within these limiting values:  $0.5 < FUV - NUV < 2$ ,  $NUV - R < 2$ , and  $NUV < 21$ . The process, as done by Bianchi & et al. (2007), gives an 85% success rate in comparing QSOs identified by color and those spectroscopically confirmed. This is consistent with our own results, as detailed in § 5.

This yielded a primary quasar candidate list of 97 targets (Table 2, Figure 3).

## 5 DISCOVERY SPECTRA

We obtained spectra for a handful of our candidates during unrelated observing runs in Winter 2008 at the Keck and Lick Obser-

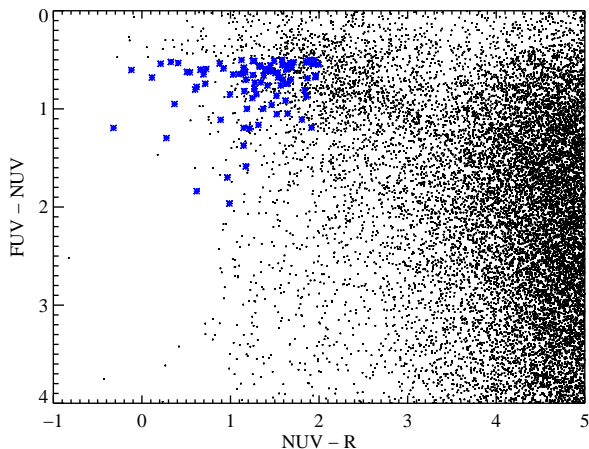


**Figure 3.** Color-color diagram of all extracted objects detected in each of our  $FUV$ ,  $NUV$ , and KPNO/ $R$  imaging (AB magnitudes). QSO candidates (blue) were determined by location in color-color space and with  $NUV$  and  $FUV < 21$ . The black dots that lie in the region of color-color space occupied by our preferred QSO candidates do not satisfy our brightness criteria ( $NUV < 21$ ).

**Table 4.** Lick/KAST Spectroscopy of QSO Candidates

Name	$\alpha_{GALEX}$ (J2000)	$\delta_{GALEX}$ (J2000)	Date (UT)	Exp. (s)
J000817+400223	00:08:17	+40:02:23	28Sep2008	600
J000825+400345	00:08:25	+40:03:45	28Sep2008	600
J001036+400314	00:10:36	+40:03:14	25Sep2008	600
J001117+402202	00:11:17	+40:22:02	26Sep2008	800
J001502+412756	00:15:02	+41:27:56	28Sep2008	600
J001553+412026	00:15:53	+41:20:26	25Sep2008	600
J001601+411820	00:16:01	+41:18:20	29Sep2008	720
J001632+414752	00:16:32	+41:47:52	26Sep2008	800
J001836+411611	00:18:36	+41:16:11	28Sep2008	300
J002007+450802	00:20:07	+45:08:02	26Sep2008	900

[The complete version of this table is in the electronic edition. The printed edition contains only a sample.]

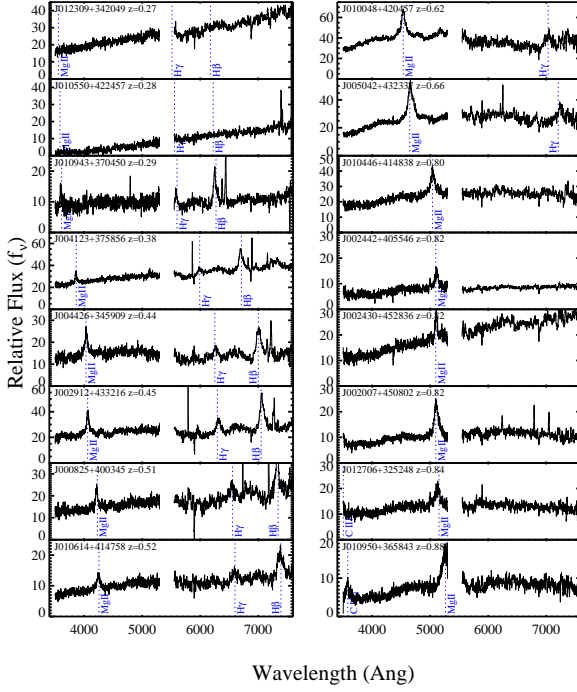
vatories with the LRIS (Oke et al. 1995) and Kast spectrometers respectively. Several of these spectra revealed extragalactic sources including two AGN. We then initiated a spectroscopic follow-up campaign at Lick Observatory. The first results of this survey are presented here.

Table 4 summarizes the observations of QSO candidates obtained during a five night run at Lick Observatory (September 25–29, 2008). These were drawn primarily from the candidate list given in Table 2, but were supplemented by targets with slightly less stringent color criteria. For all observations we used the Kast spectrograph mounted on the Lick 3m telescope. The instrument was configured with the  $2''$ -wide slit and the D55 dichroic that split the light into the blue and red cameras. We employed the 452/3306 grism on the blue side giving a  $FWHM \approx 2.8\text{\AA}$  spectral resolution for wavelengths spanning 3300–5400 $\text{\AA}$ . On the red side, we used the 600/7500 grating tilted to provide coverage from 5600–8000 $\text{\AA}$  with a  $FWHM \approx 4.6\text{\AA}$  spectral resolution. We took spectral images of Ar, He, Cd, and quartz lamps for wavelength calibration and flat-fielding.

**Table 5.** UV Bright, Extragalactic Sources Behind M31

Name	$\alpha_{GALEX}$ (J2000)	$\delta_{GALEX}$ (J2000)	$\rho_{M31}^a$ (kpc)	$FUV$ (AB)	$NUV$ (AB)	$z$
AGN (Broad Emission Lines)						
J000825+400345	00:08:25	+40:03:45	90	19.14	18.78	0.51
J001632+414752	00:16:32	+41:47:52	67	20.53	19.97	1.98
J002007+450802	00:20:07	+45:08:02	77	20.93	19.09	0.82
J002026+451251	00:20:26	+45:12:51	77	20.36	19.54	1.25
J002153+452422	00:21:53	+45:24:22	77	20.83	18.86	0.89
J002209+452453	00:22:09	+45:24:53	76	20.98	20.32	0.93
J002430+452836	00:24:30	+45:28:36	73	20.63	19.97	0.82
J002442+405546	00:24:42	+40:55:46	47	20.80	19.22	0.82
J002742+451458	00:27:42	+45:14:58	66	19.24	18.45	0.97
J002912+433216	00:29:12	+43:32:16	46	19.22	18.96	0.45
J003132+372752	00:31:32	+37:27:52	60	19.83	19.10	1.32
J003407+373520	00:34:07	+37:35:20	55	20.37	19.32	1.33
J004123+375856	00:41:23	+37:58:56	45	19.14	18.73	0.38
J004133+352619	00:41:33	+35:26:19	80	19.77	19.06	0.89
J004207+364255	00:42:07	+36:42:55	62	20.81	19.65	1.50
J004426+345909	00:44:26	+34:59:09	86	19.39	19.10	0.44
J005042+432337	00:50:42	+43:23:37	35	19.71	18.71	0.66
J005117+432160	00:51:17	+43:21:60	36	20.48	19.37	1.40
J005305+391453	00:53:05	+39:14:53	39	20.89	19.69	1.00
J005617+393437	00:56:17	+39:34:37	42	19.98	19.06	1.13
J010048+420457	01:00:48	+42:04:57	47	19.67	18.78	0.62
J010446+414838	01:04:46	+41:48:38	57	19.71	18.51	0.80
J010452+450843	01:04:52	+45:08:43	76	20.14	19.38	1.37
J010550+422457	01:05:50	+42:24:57	61	19.70	19.18	0.28
J010614+414758	01:06:14	+41:47:58	60	20.34	19.72	0.52
J010943+370450	01:09:43	+37:04:50	91	19.86	19.63	0.29
J010950+365843	01:09:50	+36:58:43	92	20.87	19.49	0.88
J012122+343640	01:21:22	+34:36:40	137	20.21	19.17	1.52
J012309+342049	01:23:09	+34:20:49	143	19.24	18.91	0.27
J012706+325248	01:27:06	+32:52:48	165	19.78	19.35	0.84
J012903+320817	01:29:03	+32:08:17	176	20.56	19.56	1.11
Galaxies (Narrow Emission Lines)						
J000817+400223	00:08:17	+40:02:23	91	19.38	18.94	0.045
J001036+400314	00:10:36	+40:03:14	85	19.23	18.68	0.033
J001117+402202	00:11:17	+40:22:02	82	20.83	19.96	0.085
J001553+412026	00:15:53	+41:20:26	69	19.53	19.03	0.048
J001601+411820	00:16:01	+41:18:20	68	19.68	19.31	0.069
J002541+423336	00:25:41	+42:33:36	47	20.63	20.11	0.138
J004126+445652	00:41:26	+44:56:52	50	20.66	20.03	0.092
J004144+460148	00:41:44	+46:01:48	65	20.67	19.79	0.114
J004222+350017	00:42:22	+35:00:17	85	20.57	20.01	0.067
J004301+445242	00:43:01	+44:52:42	49	20.34	19.79	0.090
J004307+355523	00:43:07	+35:55:23	73	20.20	19.66	0.110
J004440+360333	00:44:40	+36:03:33	71	19.89	19.37	0.054
J004502+355727	00:45:02	+35:57:27	73	19.92	19.46	0.027
J005651+395237	00:56:51	+39:52:37	41	20.66	19.98	0.070
J005754+414153	00:57:54	+41:41:53	39	20.71	20.04	0.090
J005758+405834	00:57:58	+40:58:34	39	20.76	20.26	0.083
J005832+423847	00:58:32	+42:38:47	44	20.65	20.04	0.089
J005948+405227	00:59:48	+40:52:27	44	20.86	20.36	0.079
J010227+402643	01:02:27	+40:26:43	52	20.73	20.19	0.252
J010552+363321	01:05:52	+36:33:21	89	20.69	19.95	0.126
J011324+414531	01:13:24	+41:45:31	79	20.75	20.15	0.101
J011436+415018	01:14:36	+41:50:18	82	20.96	20.38	0.133
J011619+414737	01:16:19	+41:47:37	86	20.91	20.16	0.121
J012436+325122	01:24:36	+32:51:22	161	19.83	19.13	0.109
J012950+324441	01:29:50	+32:44:41	172	18.54	18.04	0.046
J013010+321151	01:30:10	+32:11:51	178	20.79	20.26	0.076
J013021+321336	01:30:21	+32:13:36	178	20.97	20.12	0.046
J013033+320958	01:30:33	+32:09:58	179	20.37	19.75	0.136
J013036+320859	01:30:36	+32:08:59	179	19.54	18.94	0.021





**Figure 4.** Lick/Kast discovery spectra of UV-bright AGN and quasars in the field surrounding M31. The data at  $\lambda < 5400\text{\AA}$  ( $> 5600\text{\AA}$ ) correspond to the blue (red) camera of the Kast spectrometer. The gap at  $\lambda \approx 5400 - 5500\text{\AA}$  corresponds to the central wavelength of the dichroic used in the observations. The dotted vertical lines show the positions of prominent emission lines for AGN, shifted according to the measured redshift.

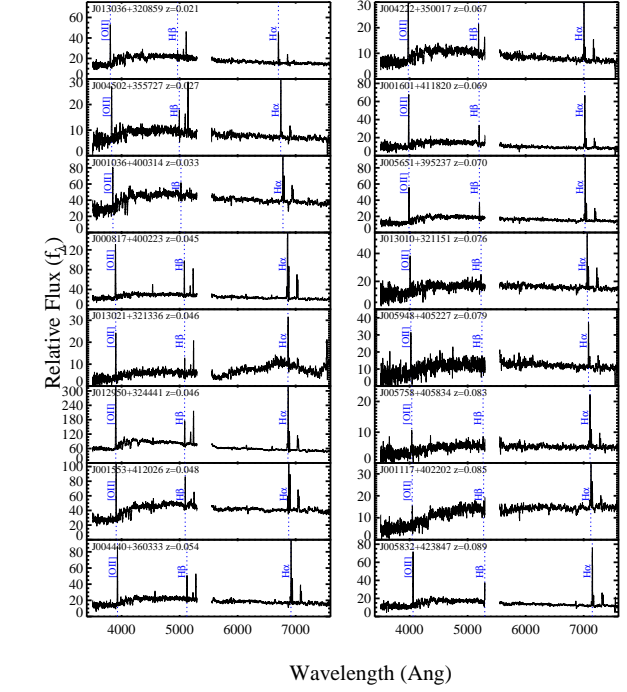
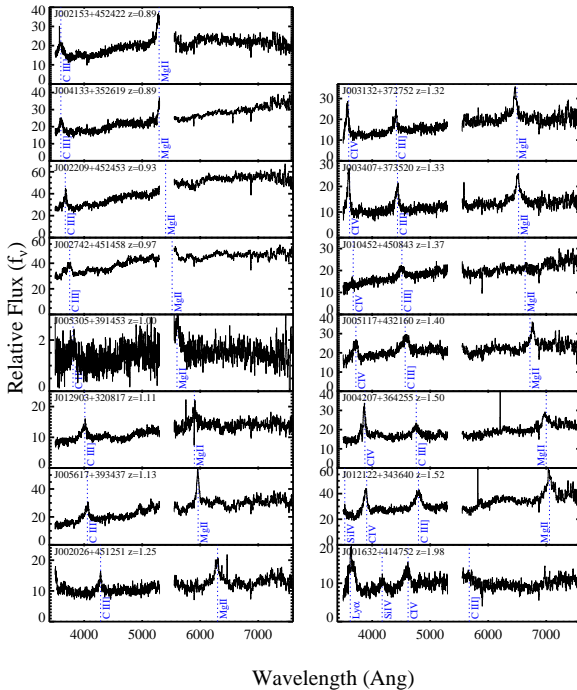
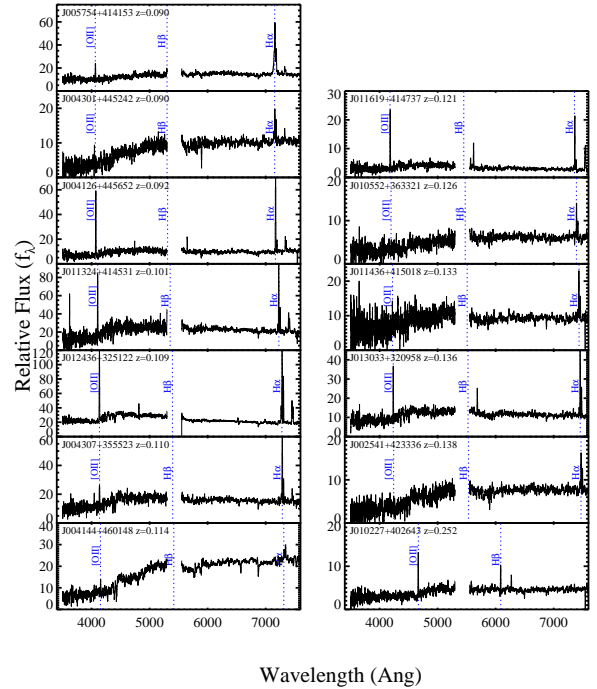


**Figure 5.** Same as Figure 4 but for extragalactic objects showing only narrow emission lines, presumed to be star-forming galaxies.



The data were reduced with the LowRedux<sup>3</sup> package developed by J. Hennawi, S. Burles, and JXP that is bundled within the XIDL<sup>4</sup> software package. The data were flat fielded to remove pixel-to-pixel variations, wavelength calibrated, sky subtracted, and

<sup>3</sup> <http://www.icolick.org/~xavier/LowRedux/index.html>

<sup>4</sup> <http://www.icolick.org/~xavier/IDL/>

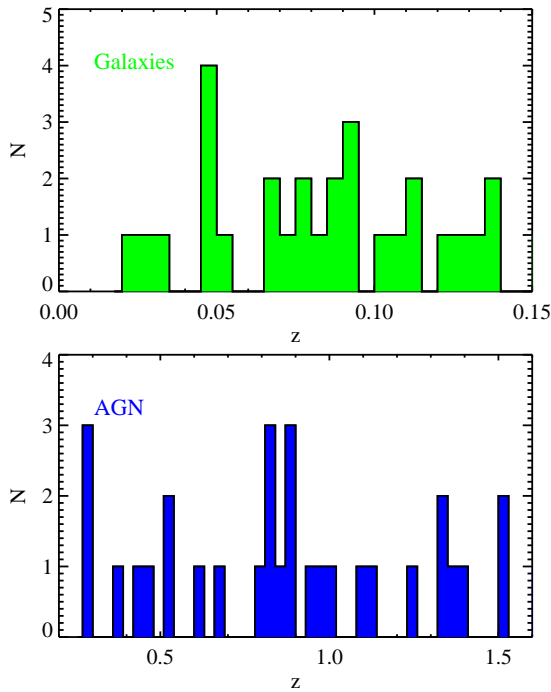


**Figure 6.** Spectroscopic redshifts for the 60 extragalactic sources discovered in our survey. The redshift range of each panel has been truncated for presentation purposes.

optimally extracted. The 1D spectra were corrected for instrumental flexure and then flux calibrated using a sensitivity function derived from observations of a spectrophotometric standard taken the first night. All nights were clear and likely to have been nearly photometric. The absolute flux calibration of the data is not accurate because of slit losses but we estimate the relative fluxing is accurate to within  $\approx 20\%$ . For targets with multiple exposures, we coadded the 1D spectra after weighting by the median inverse variance.

Each 1D spectrum of our quasar candidates was visually analyzed for significant absorption and emission lines to perform object classification. The principle contaminants to the quasar candidates are: (i) foreground Galactic stars that show prominent Balmer absorption lines and (ii) star-forming galaxies that exhibit narrow emission lines and occasional CaH+K and Balmer absorption lines. In nearly every spectrum, we identified multiple emission and/or absorption features which unambiguously classified the object and yielded an estimate of the target’s redshift. All of the extragalactic sources are listed in Table 5. We characterize objects with narrow emission lines as galaxies and report all others as AGN (many of these may be more properly classified as quasars). There is one source (J012309+342049) that exhibits a nearly featureless spectrum across our full wavelength coverage. The absence of Balmer absorption features rules out this target as a Galactic star. We initially classified it as an unknown extragalactic source and suspected it to be a blazar. Indeed, a search using SIMBAD revealed this source was previously known as a BL Lacertae object at  $z = 0.27$  (Perlman et al. 1996). One of the other AGN was also previously discovered using X-ray imaging (J002742+451457; Xie et al. 1997). Spectra of all the extragalactic sources are shown in Figures 4 and 5.

Of the targets drawn from our primary candidate list for spectroscopic study (59 total from Table 2), 85% were verified as ex-

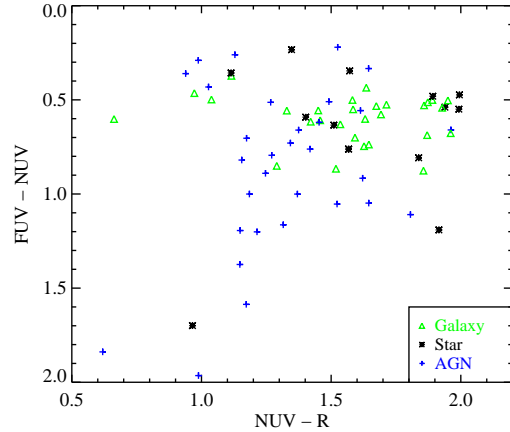


**Figure 7.** Color-color plot of the 76 objects targeted for follow-up optical spectroscopy. The sources spectroscopically classified as AGN show systematically redder  $FUV - NUV$  color and bluer  $NUV - R$  than the galaxy and stars.

tragalactic and half of these show broad-lines indicating strong AGN activity. The redshift distributions of the objects are given in Figure 6. The galaxies discovered by our survey are generally blue, faint star-forming systems with typical late-type spectra. A significant number of the higher redshift systems, however, have red continua and exhibit absorption lines characteristic of early-type systems. We interpret their significant UV fluxes as signatures of the so-called “UV upturn” observed in early-type galaxies (e.g. O’Connell 1999).

Regarding the stellar contaminants, the majority of these were especially bright ( $R < 17$  mag) and could have been avoided by imposing a brightness limit to the candidate criteria. On the other hand, if any of these had been confirmed as AGN they would have been especially valuable as probes of M31’s halo. Figure 7 shows that the targets classified as AGN have systematically redder  $FUV - NUV$  color and systematically bluer  $NUV - R$  colors than the typical galaxies observed. By restricting the pre-selection to  $FUV - NUV > 0.5$  and  $NUV - R < 1.4$ , one would likely increase the efficiency of quasar selection. The cut on  $FUV - NUV$  color, however, would also reduce the number of candidates with higher  $FUV$  flux. We plan for a future observing run in Fall 2009 to confirm additional candidates.

## 6 SUMMARY

Adopting color-color criteria based on KPNO/ $R$ , GALEX/ $NUV$ , and GALEX/ $FUV$  photometry, we have culled a list of  $\approx 100$  quasar candidates (Table 2) from 50 deg<sup>2</sup> out to 150 kpc. We have obtained follow-up spectroscopy for 59 of these “tier 1” candidates and an additional 27 objects with less restrictive color-color criteria. We report the detection of 30 broad-lined targets which we classify as AGN and one featureless source which is a previously known blazar. We also report on 29 galaxies ranging from  $z = 0.02$  to  $z = 0.25$ .

The AGN are distributed across M31’s halo with impact parameters ranging from 35 to 180 kpc (Figure 8). Roughly half of these sources are sufficiently bright for follow-up UV spectroscopy using the HST/COS spectrometer, albeit with multi-orbit expo-



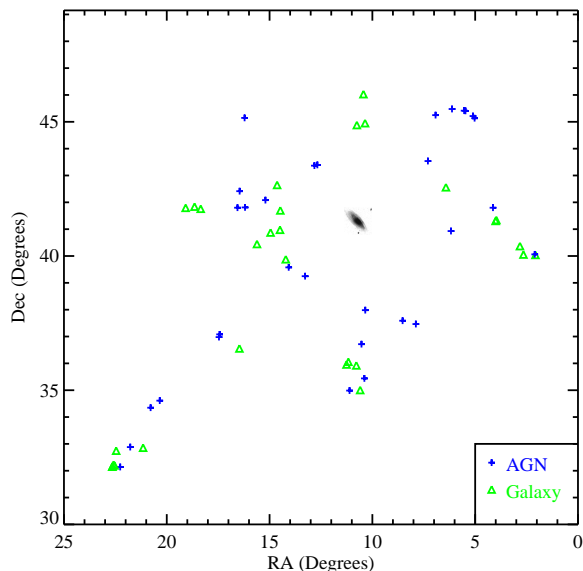


**Figure 8.** Projected distribution of extragalactic sources in the field surrounding M31 discovered or rediscovered (2 sources) by our survey to date. The AGN, which are optimal for follow-up absorption-line spectroscopy of M31’s halo, are distributed through the projected halo with impact parameters ranging from  $\approx 35 - 180$  kpc.

tures. Such spectra could be used to examine the spatial distribution of enriched gas via absorption-line analysis of transitions like  $Si_{II}$  1260,  $Si_{IV}$  1393, 1402, and  $C_{IV}$  1548, 1550, revealing the metallicity, gas kinematics, molecular content, and the nature of M31’s ionized gas. As the identified QSOs are distributed throughout M31, the sampling of this gas content directly aids in our understanding of galaxy formation processes through the deconvolution of disc/halo regions and the interpretation of accretion events such as the giant southern stream. Recent work has characterized the properties and distribution of stars across these regions of M31, but an unambiguous separation of the components requires a sampling of the gas dynamics.

Future surveys (e.g., PAndAS and PAndromeda) will soon lead to global maps of M31 and we can target future QSO surveys to interesting regions with/without substructure. The area that is covered by our GALEX pointings is small relative to the (yet) unobserved M31 halo through optical imaging.

Various surveys of M31, most notably the SDSS, have revealed many QSO detections, but focused on the disc itself. This project used those tools to extend the search to the newly discovered halo of M31. Future searches for quasars toward M31 in pointings not covered by this survey could provide an additional hundred or more targets for such analysis.

## ACKNOWLEDGMENTS

AF, JXP JSK, and PG acknowledge support NASA grant NNG06GD37G, as part of the GALEX GO program. PG and JSK acknowledge support from NSF grant AST-0607852. J. S. was supported by NASA through a Hubble Fellowship, administered by the Space Telescope Science Institute, which is operated by the As-

sociation of Universities for Research in Astronomy, Incorporated, under NASA contract NAS5-26555.

## REFERENCES

- Allen S. W., Rapetti D. A., Schmidt R. W., Ebeling H., Morris R. G., Fabian A. C., 2008, *MNRAS*, 383, 879
- Atlee D. W., Gould A., 2007, *ApJ*, 664, 53
- Bertin E., Arnouts S., 1996, *Astronomy and Astrophysics Supplement*, 117, 393
- Bianchi L., et al. 2007, *ApJS*, 173, 659
- Brown T. M., Smith E., Ferguson H. C., Guhathakurta P., Kalirai J. S., Rich R. M., Renzini A., Sweigart A. V., Reitzel D., Gilbert K. M., Geha M., 2007, *ApJ*, 658, L95
- Chen H.-W., Lanzetta K. M., Webb J. K., 2001, *ApJ*, 556, 158
- Chen H.-W., Prochaska J. X., 2000, *ApJ*, 543, L9
- Chen H.-W., Tinker J. L., 2008, *ArXiv e-prints*, 801
- Churchill C. W., Mellon R. R., Charlton J. C., Jannuzi B. T., Kirhakos S., Steidel C. C., Schneider D. P., 2000, *ApJS*, 130, 91
- Dekel A., Birnboim Y., Engel G., Freundlich J., Goerdt T., Muncuoglu M., Neistein E., Pichon C., Teyssier R., Zinger E., 2008, *ArXiv e-prints*
- Forman W., Jones C., 1982, *ARA&A*, 20, 547
- Fukugita M., Hogan C. J., Peebles P. J. E., 1998, *ApJ*, 503, 518
- Gilbert K. M., Fardal M., Kalirai J. S., Guhathakurta P., Geha M. C., Isler J., Majewski S. R., Ostheimer J. C., Patterson R. J., Reitzel D. B., Kirby E., Cooper M. C., 2007, *ApJ*, 668, 245
- Gilbert K. M., Guhathakurta P., Kalirai J. S., Rich R. M., Majewski S. R., Ostheimer J. C., Reitzel D. B., Cenarro A. J., Cooper M. C., Luine C., Patterson R. J., 2006, *ApJ*, 652, 1188
- Guhathakurta P., Ostheimer J. C., Gilbert K. M., Rich R. M., Majewski S. R., Kalirai J. S., Reitzel D. B., Patterson R. J., 2005, *arXiv preprint (astro-ph/0502366)*
- Guhathakurta P., Rich R. M., Reitzel D. B., Cooper M. C., Gilbert K. M., Majewski S. R., Ostheimer J. C., Geha M. C., Johnston K. V., Patterson R. J., 2006, *AJ*, 131, 2497
- Hogg D. W., Blanton M., Lang D., Mierle K., Roweis S., 2008, in Argyle R. W., Bunclark P. S., Lewis J. R., eds, *Astronomical Data Analysis Software and Systems XVII Vol. 394 of Astronomical Society of the Pacific Conference Series*, Automated Astrometry (Invited). pp 27+–
- Ibata R., Martin N. F., Irwin M., Chapman S., Ferguson A. M. N., Lewis G. F., McConnachie A. W., 2007, *ApJ*, 671, 1591
- Kacprzak G. G., Churchill C. W., Steidel C. C., Ceverino D., Klypin A. A., Murphy M. T., 2007, *ArXiv e-prints*, 710
- Kalirai J. S., Gilbert K. M., Guhathakurta P., Majewski S. R., Ostheimer J. C., Rich R. M., Cooper M. C., Reitzel D. B., Patterson R. J., 2006, *ApJ*, 648, 389
- Kereš D., Katz N., Weinberg D. H., Davé R., 2005, *MNRAS*, 363, 2
- Lanzetta K. M., Bowen D. V., 1992, *ApJ*, 391, 48
- Morrissey P., GALEX Science Team 2005, in *Bulletin of the American Astronomical Society Vol. 37 of Bulletin of the American Astronomical Society, A Flight Performance Update for the Galaxy Evolution Explorer (GALEX)*. pp 1454+–
- Mulchaey J. S., Davis D. S., Mushotzky R. F., Burstein D., 1996, *ApJ*, 456, 80
- Mulchaey J. S., Davis D. S., Mushotzky R. F., Burstein D., 2003, *ApJS*, 145, 39
- O’Connell R. W., 1999, *ARA&A*, 37, 603

- Oke J. B., Cohen J. G., Carr M., Cromer J., Dingizian A., Harris F. H., Labrecque S., Lucinio R., Schaal W., Epps H., Miller J., 1995, *PASP*, 107, 375
- Perlman E. S., Stocke J. T., Schachter J. F., Elvis M., Ellingson E., Urry C. M., Potter M., Impey C. D., Kolchinsky P., 1996, *ApJS*, 104, 251
- Prochaska J. X., Tumlinson J., 2008, *ArXiv e-prints*
- Stetson P. B., 1994, *PASP*, 106, 250
- Thilker D. A., Braun R., Walterbos R. A. M., Corbelli E., Lockman F. J., Murphy E., Maddalena R., 2004, *ApJ*, 601, L39
- Tripp T. M., Sembach K. R., Bowen D. V., Savage B. D., Jenkins E. B., Lehner N., Richter P., 2007, *ArXiv e-prints*, 706
- Xie G., Cha G., Bai J., Li K., Brinkmann W., 1997, *Acta Astrophysica Sinica*, 17, 437
- Zibetti S., Ménard B., Nestor D. B., Quider A. M., Rao S. M., Turnshek D. A., 2007, *ApJ*, 658, 161